CrossMark

Investigation of Gas and Liquid Multiphase Flow in the Rheinsahl–Heraeus (RH) Reactor by Using the Euler–Euler Approach

GUJUN CHEN,[1] SHENGPING HE,[1,2] YUGANG LI,[1] YINTAO GUO,[1] and QIAN WANG[1]

1.—College of Materials Science and Engineering, Chongqing University, Chongqing 400044, China. 2.—e-mail: heshp@cqu.edu.cn

In the present work, a mathematical model was developed to understand the multiphase flow behavior in a Rheinsahl–Heraeus (RH) reactor by using the Euler–Euler approach, and the effects of initial bubble diameter, nonequilibrium expansion of bubble caused by sudden thermal effect and sharp pressure drop, and various interphase forces were considered and clarified. The simulation results of mixing time, liquid circulation rate, and local liquid velocity in RH agree well with the measured results. The result indicates that the initial bubble diameter has a weak impact on the multiphase flow but that the bubble expansion has a tremendous impact on it for an actual RH. Meanwhile, the drag force and turbulent dispersion force strongly influence the multiphase flow, whereas the lift force and virtual mass force only have negligible influence on it. Furthermore, the turbulent dispersion force should be responsible for reasonable prediction of multiphase flow behavior in the RH reactor.

INTRODUCTION

During production of low-carbon and ultra-low-carbon steels, the Rheinsahl–Heraeus (RH) reactor plays a crucial role in the refining process for removing the hydrogen, carbon, and inclusions from molten steel and homogenizing the components and temperature of steel.[1–4] The achievement of these functions is dependent on the flow field present in the RH reactor. Therefore, to accelerate the refining efficiency, it is necessary to investigate the characteristics of fluid flow and mixing behavior in the RH reactor. As illustrated in Fig. 1, RH refining begins with lifting the ladle or reducing the vacuum chamber until immersing snorkels in the melt. Then, the melt will be suctioned into the snorkels and occupy the lower part of the vacuum chamber through reducing the pressure in the vacuum chamber to an extreme value. After that, compressed argon is blown into the up-snorkel through nozzles, which causes the melt to recirculate between a vacuum chamber and a ladle.

It is widely accepted that the refining efficiency can be promoted when the circulation flow rate increases and the mixing time decreases.[3,5]

Because it is impossible to measure the circulation rate of the actual RH reactor directly, few measurements of mixing time have been conducted to predict the circulation rate.[6,7] For the same reason, some formulas based on water modeling have been proposed to calculate the circulation rate and mixing time in the actual RH reactor.[8,9] However, there are many problems when the results of water modeling are applied to an actual RH reactor as a result of the significant difference of conditions. In 1975 and 1983, Nakanishi[6] and Shirabe,[1] respectively, proposed a two-dimensional mathematical model by specifying the melt velocity at the end of snorkels, in which the vacuum chamber and gas phase were ignored and short circuiting of flow between the snorkels was observed. In the same way, three-dimensional methods were developed to simulate the melt flow only in the ladle of the RH reactor by many researchers,[7,10–12] in which no short circuiting was observed. Gas–liquid multiphase flow in the up-snorkel plays a decisive function in determining the characteristics of circulation and mixing in the RH reactor, so it is not appropriate to neglect the vacuum chamber and gas phase. Later, based on the homogeneous fluid
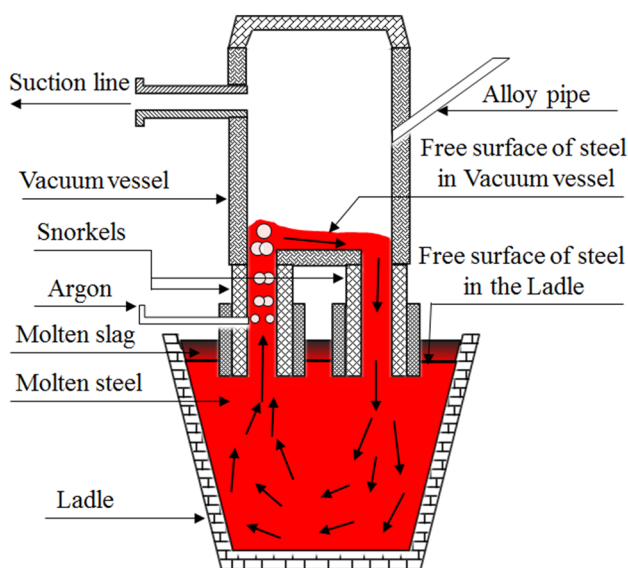
Fig. 1. Schematic diagram of an RH reactor.

model, numerous authors[13–19] investigated the fluid flow of the whole RH reactor. In these models, to calculate the buoyancy force acting on gas, which was added in momentum equation as a source term, the shape and position of the gas–liquid multiphase region (plume zone) were considered. However, the shape and position of the plume must be prespecified and normally obtained from empirical correlations, which also limits their application. More importantly, these empirical correlations were obtained experimentally under a single nozzle;[20–23] nevertheless, a big difference of the gas-holdup distribution and plume shape were observed between multiple nozzles and a single nozzle in the case of horizontal gas blowing.[24]

To overcome the shortcomings with the homogeneous fluid model, multiphase models, i.e., Eulerian–Lagrangian and Eulerian–Eulerian approaches,[25–29] were put forward. In the Euler–Lagrange approach, liquid is treated as a continuum by solving the Navier–Stokes equations, whereas gas is solved by tracking a large number of bubbles through the calculated flow field. As demonstrated by Kishan,[25] the predicted circulation rate with this approach for water modeling was considerably less than observation. Actually, the Euler–Lagrange approach requires that the gas-holdup is generally less than 12%.[30] Thus, this approach may not be appropriate for treating the behavior of gas-liquid flow in the RH reactor because of the higher gas-holdup in the plume zone.[31] Cournil et al.[32] also suggested that compared with the Eulerian–Lagrangian approach, the Euler–Euler approach should be a better choice to obtain a precise result for the RH reactor.

In the Euler–Euler approach, the continuation and momentum equations are satisfied by each phase individually, and both phases are coupled by interphase forces. Recently, some authors[22,33–41] investigated the multiphase flow in the RH reactor with the Euler–Euler approach. However, compared with the experimental results, predictions were still far from satisfactory. For water modeling, predicted values at different gas flow rates were consistently lower than the experimental values with an error of about 15% to 20%, as reported by Kishan.[35] Interestingly, opposite results were found in the study of Sheng et al.,[38,39] in which predictions under a different gas flow rate were always higher than the experiments with an error of 10–15%. Also, the predictions of the water circulation rate by Parreiras et al.[36,37] were close to the experimental results only at a narrow range of the gas flow rate. In addition, based on the Euler–Euler approach, the gas-adhering wall effect[33] was observed by most research,[22,33–37,40,41] whereas this phenomenon was absent in individual studies[38,39] regardless of water modeling or the actual RH reactor. Obviously, the large differences among different investigations mainly came from the consideration of various interphase forces. Unfortunately, almost no author investigated the influence of various interphase forces on multiphase flow in the RH reactor, although these forces have been fully developed in a number of fundamental studies.[42,43] Compared with water modeling, there were more problems waiting to be solved for the actual RH reactor. The most serious problem was how to consider the nonequilibrium expansion of bubble caused by a sudden thermal effect and sharp pressure drop in the rising process of argon in the melt. By using the Euler–Euler approach, Kishan[35] calculated the circulation rate in an actual RH reactor and found that the predicted value was much lower compared with the value in the actual plant, as a result of the neglect of bubble expansion.[35] Hence, Kishan[25,35] proposed that gas expansion must be considered, and this was also realized by Parreiras et al.[36,37] However, this was neglected by all the researchers[22,33–41] who studied the multiphase flow in an actual RH reactor with the Euler–Euler approach.

In general, it can be concluded that, for the Euler–Euler approach, the key factors that affect accurate prediction of multiphase flow in the RH reactor are the consideration of gas expansion and the reasonable inclusion of various interphase forces. Therefore, the aim of the present work is to develop a mathematical model to reasonably describe the multiphase flow in an RH reactor based on the Euler–Euler approach. The simulation results of mixing time, liquid circulation rate, and local liquid velocity are compared with the measured data. Meanwhile, the effects of the initial

bubble diameter, bubble expansion, and various interphase forces on the multiphase flow in the RH reactor are investigated.

MATHEMATICAL MODEL

The multiphase flow in the RH reactor has been solved with the Euler–Euler approach based on the following assumptions:

a. Both phases are Newtonian and viscous;[33,44] the liquid phase is incompressible.[35,44]
b. The effect of slag on fluid flow is neglected;[35,44,45] fluid flow is at steady state.[35,44,45]
c. Bubbles are assumed to be spherical.[22,25,33]
d. Many models for bubble breakup and coalescence are available in chemical engineering literatures.[46–48] However, none of them have been validated for the argon–steel system in metallurgy. In previous literatures,[22,25,33,35] the coalescence and breakup of bubbles, and the interactions among bubbles, are completely neglected, and the same assumption was made here.
e. In the present work, gas expansion caused by thermal and pressure effects is considered for the actual RH reactor; that is, the injected gas will absorb heat from melt. For bubbles, the absorbed energy is enough to heat bubbles from room temperature to melt temperature. Thus, the gas properties must be treated as a function of temperature and pressure. However, for melt, the temperature drop caused by bubble absorbing is small, which is not enough to influence the melt properties notably. So, the melt temperature is assumed to keep constant (1873 K).

Governing Equations

Mass conservation:

$$\frac{\partial}{\partial t}(\alpha_i \rho_i) + \nabla \cdot (\alpha_i \rho_i \vec{u}_i) = 0 \tag{1}$$

α_i, ρ_i, and $\vec{u}_i$ are the volume fraction, density, and phase-averaged velocity vector of liquid $(i = l)$ and gas $(i = g)$, respectively. A constraint condition $(\alpha_g + \alpha_l = 1)$ is satisfied to enclose the model.

Momentum conservation:

$$\frac{\partial}{\partial t}(\alpha_i \rho_i \vec{u}_i) + \nabla \cdot (\alpha_i \rho_i \vec{u}_i \vec{u}_i)$$
$$= -\alpha_i \nabla p + \nabla \cdot \left[\alpha_i (\mu_l + \mu_{t,l}) \left(\nabla \vec{u}_i + (\nabla \vec{u}_i)^T \right) \right] \tag{2}$$
$$+ \alpha_i \rho_i \vec{g} + \vec{F}_i$$

$\vec{g}$ is the gravitational acceleration vector, μ_l is the liquid viscosity, and $\mu_{t,l}$ is the turbulent viscosity of liquid, which can be determined by a k–ε dispersed turbulence model. p is the pressure, and $\vec{F}_i$ is the interaction force between two phases:

$$\vec{F}_l = -\vec{F}_g = \vec{F}_{drag} + \vec{F}_{lift} + \vec{F}_{vm} + \vec{F}_{td} \tag{3}$$

where the terms on the right side of Eq. 3 denote the drag force ($\vec{F}_{drag}$), lift force ($\vec{F}_{lift}$), virtual mass force ($\vec{F}_{vm}$), and turbulent dispersion force ($\vec{F}_{td}$), respectively.

Drag Force

For gas-stirred multiphase flow in the RH reactor, drag will tend to slow the fast-moving bubble and will speed up the surrounding liquid due to viscous dissipation. Generally, the drag force is the dominant contribution to the interaction forces, which is described as follows:

$$\vec{F}_{drag} = K_{gl}(\vec{u}_g - \vec{u}_l) \tag{4}$$

K_{gl} is the interphase exchange coefficient:

$$K_{gl} = C_D \frac{3\alpha_g \alpha_l \rho_l}{4 d_g} |\vec{u}_g - \vec{u}_l| \tag{5}$$

d_g is the bubble diameter, and C_D is the drag coefficient, which can be estimated from the model of Schiller and Naumann[49] and has been widely used to model gas–liquid flow for a spherical bubble:[50–52]

$$C_D = \max\left(24\left(1 + 0.15 \mathrm{Re}^{0.687}\right)/\mathrm{Re},\ 0.44\right) \tag{6}$$

$$\mathrm{Re} = \frac{\rho_l |\vec{u}_g - \vec{u}_l| d_g}{\mu_l} \tag{7}$$

Lift Force

The lift force acts on a bubble mainly caused by the existence of velocity gradient in the flow field of liquid, which is perpendicular to the main flow direction:[53,54]

$$\vec{F}_{lift} = -C_L \rho_l \alpha_g (\vec{u}_g - \vec{u}_l) \times (\nabla \times \vec{u}_l) \tag{8}$$

C_L is the lift coefficient, which typically has a value of 0.5 for the spherical bubble.[35]

Virtual Mass Force

The virtual mass effect can occur when a bubble accelerates relative to the liquid, which can be defined as follows:[53]

$$\vec{F}_{vm} = C_{VM} \alpha_g \rho_l \left(\frac{d_l \vec{u}_l}{dt} - \frac{d_g \vec{u}_g}{dt} \right) \tag{9}$$

The term $\frac{d_i}{dt}$ denotes the phase material time derivative of the form $\frac{d_i(\vec{u}_i)}{dt} = \frac{\partial(\vec{u}_i)}{\partial t} + (\vec{u}_i \cdot \nabla)\vec{u}_i$ and C_{VM} is the virtual mass coefficient, which typically has a value of 0.5 for a spherical bubble.[35]

Turbulent Dispersion Force

The turbulent dispersion force can act on a bubble due to the turbulent fluctuation of liquid:

$$\vec{F}_{td} = -K_{gl}\vec{u}_{drift} \tag{10}$$

$\vec{u}_{drift}$ is the drift velocity:[55]

$$\vec{u}_{drift} = -\frac{D_{t,gl}}{\sigma_{gl}} \cdot \left(\frac{\nabla\alpha_g}{\alpha_g} - \frac{\nabla\alpha_l}{\alpha_l}\right) \tag{11}$$

σ_{gl} is the dispersion Prandtl number, which can be set as 0.75.[55] $D_{t,gl}$ is the turbulent dispersion coefficient.[56]

Bubble Properties

Several formulas were proposed to calculate the initial bubble diameter, $d_{g,0}$, formed at the nozzle tip,[25,57–59] and a reasonable result could be achieved for the RH reactor by using the correlation reported by Sano:[31,60]

$$d_{g,0} = 0.091\left(\frac{\sigma_l}{\rho_l}\right)^{0.5} u_{g,0}^{0.44} \tag{12}$$

σ_l is the surface tension, N/m, and $u_{g,0}$ is the gas velocity at the nozzle exit, m/s.

In the actual RH reactor, the difference between the pressure of the vacuum chamber and the pressure at the nozzle is so large that the argon expansion caused by a pressure drop should be considered. Meanwhile, the argon will be heated by high-temperature melt, which also gives rise to the sudden expansion. When rapid growth of the bubble in liquid occurs, the pressure inside the bubble is much larger than that at the surface because a pressure gradient is required to accelerate the surrounding liquid.[61] In addition, the rising time of the bubble in melt is only about 1 s in the RH reactor. Therefore, it is impossible to obtain an equilibrium expansion. For the water model, air expansion is ignored due to the normal temperature and small pressure difference.

Szekely et al.[62] presented a formula with respect to the size of the rising bubble under reduced pressure, and it was modified by Park[14] to consider the thermal effect:

$$\frac{d^2r_g}{dt^2} + \frac{3}{2r_g}\left(\frac{dr_g}{dt}\right)^2 = \frac{1}{\rho_l r_g}\left[P_0\left(\left(\frac{r_{g,0}}{r_g}\right)^3\left(\frac{T_g}{T_{g,0}}\right) - 1\right) + \rho_l g u_r t\right]$$

$$t = 0; \ r_g = r_{g,0}, \ \frac{dr_g}{dt} = 0, \ T_{g,0} = 300 \tag{13}$$

r_g is the bubble radius (m); T_g is the bubble temperature (K); t is the rising time of bubble (s); $r_{g,0}$ and $T_{g,0}$ are the initial radius and temperature of bubble at nozzle, respectively; P_0 is the hydrostatic pressure at nozzle (Pa); and u_r is the bubble rising velocity relative to the melt (m/s).

Szekely et al.[61] investigated the growth of bubble rising in liquid under a vacuum condition, and it was observed that despite the considerable expansion, the rising velocity of bubble was almost kept constant, due to the shape deformation from sphere to spherical-cap.[63] For simplicity, the rising velocity of the bubble was still calculated by using the following equation[63] involving the shape deformation, and this had little effect on simulation results:[45]

$$u_r = \left[\frac{4\sigma_l^2 g}{30\rho_l\mu_l}\frac{(\rho_l - \rho_g)}{\rho_l}\right]^{1/5} \tag{14}$$

Bubble temperature can be calculated by:

$$\rho_g C_g V_g \frac{dT_g}{dt} = h_g A_g(T_l - T_g) \tag{15}$$

T_l is the melt temperature (K), and V_g, A_g, and C_g are the volume (m^3), surface area (m^2), and heat capacity (J/(kg K)) of the bubble, respectively. The heat transfer coefficient (J/(m^2 s K)), h_g, can be determined according to penetration theory:[64]

$$h_g = 2\sqrt{\frac{u_r \rho_g C_g \lambda_g}{2\pi r_g}} \tag{16}$$

The heat conductivity coefficient of argon, λ_g (J/(m s K)), can be assumed as a function of temperature:[65]

$$\lambda_g = (0.0475T_g + 3.2825) \times 10^{-3} \tag{17}$$

The heat transfer coefficient could only be calculated roughly because the bubble diameter was assumed to be kept constant in penetration theory.

To describe the change in rising distance between the bubble position and the nozzle position, h, with rising time, t, the rising velocity of the bubble relative to up-snorkel, u_g (m/s), is required:

$$h = u_g t \tag{18}$$

$$u_g = u_l + u_r \tag{19}$$

u_l is the melt velocity in the up-snorkel, which can be estimated from the equation proposed by Kuwabara:[8]

$$Q_l = 1.06\,Q_g^{1/3}D^{4/3}\left(\ln\frac{P_0}{P_{vac}}\right)^{1/3} \tag{20}$$

Q_l is the melt circulation rate (m^3/s), Q_g is the gas flow rate (Nm^3/s), P_{vac} is the pressure of the vacuum chamber (Pa), and D is the snorkel diameter (m).

Thus, the bubble diameter and density can be obtained as a function of rising distance between the bubble position and the nozzle position.

Boundary Conditions

The commercial software Fluent with user-defined functions was used to solve the multiphase flow in the RH reactor, and grid sensitivity experiments were made. The geometrical parameters and material properties employed are shown in Table I. Figure 2 shows the mesh and boundary conditions.

Table I. Dimensions and material properties of RH reactor

|	Actual RH[15,66]	Water model[67]
Up/down diameter of ladle (m)	4	0.52/0.45
Bath depth (m)	3.75	0.44
Diameter of vacuum chamber (m)	2.4	0.28
Snorkel diameter (m)	0.73	0.06
Nozzle diameter (m)	0.004	0.0008
Nozzle number	12	8
Snorkel length (m)	1.7	0.3
Submerged depth (m)	0.65	0.1
Pressure of vacuum chamber (Pa)	1333.2	97900.0
Liquid density (kg/m^3)	7020	1000
Liquid viscosity (Pa s)	0.006	0.00085
Gas density at 300 K (kg/m^3)	1.623	1.25
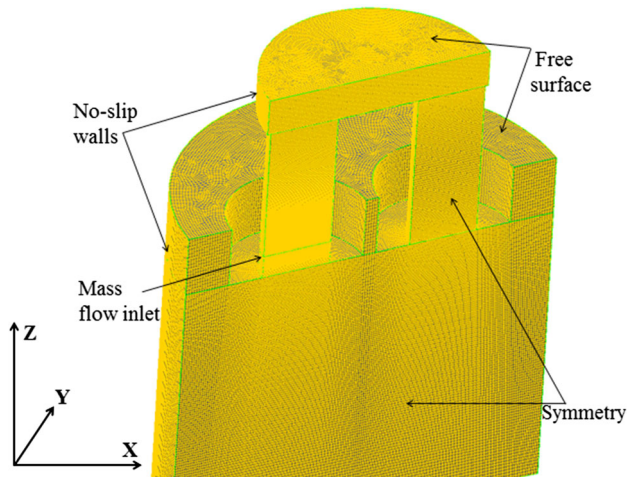
Fig. 2. Mesh and boundary conditions of an RH reactor.

Only half of the geometric model was built due to the symmetry (y = 0-mm plane) of fluid flow. The walls of the ladle, snorkels, and vacuum chamber were considered to be no-slip conditions. The standard wall function was employed for turbulent characteristic in the near-wall region. A free liquid surface was assumed at the surfaces of the ladle and vacuum chamber, where there was an outlet for gas and a free slip wall for liquid. The mass flow inlet was used for gas blowing.

RESULTS AND DISCUSSIONS

Model Validation

Calculated velocity vectors for an actual RH reactor at different sections are shown in Fig. 3 when the gas flow rate is 120 Nm^3/h. As shown, the melt in the ladle enters into the vacuum chamber through the up-snorkel due to the drive of injected gas from nozzles, and it spreads around and forms two small recirculation zones in the vacuum chamber. After that, it flows into the ladle through the down-snorkel and straightly impinges the bottom of the ladle with a high velocity; it then generates a huge recirculation zone around the downward stream in the ladle. Subsequently, the bulk of the melt flows circuitously toward the entrance of the up-snorkel, and the next circulation starts. The entire flow pattern calculated in the present work agrees well with many water modeling demonstrations[5,33,34,67] and recent simulations.[31,44,66]

To validate the present model, the computational results in the present work are compared with the experimental results reported in previous literatures.[15,66,67] In the work of Park,[15,66] 125 kg of copper was added into a 330-ton RH reactor as a tracer under three different gas flow rates. Steel samples were taken out every 12 s or 30 s, and the copper contents were analyzed to obtain the complete mixing time. The complete mixing time is defined as the time when the tracer concentration ($C(t)$) achieves the range of ±3% of the final concentration ($C(\infty)$). Figure 4 shows the calculated variation of the concentration ratio ($C(t)/C(\infty)$) with time at a gas flow rate of 120 Nm^3/h, accompanied with the measured complete mixing time.[15,66] Here, two monitoring points are located at the center of the top and bottom of the ladle, respectively. Typically, three to four circulation cycles are needed for complete mixing of the melt in the RH reactor.[5,67] Similar to the result reported by Ajmani et al.,[7] the tracer concentration at the top has three peaks before it achieves a steady value compared to the concentration variation at the bottom, which has four peaks. Clearly, it can be found in Fig. 4 that the predicted complete mixing time and the measured result match very well.

In the work of Park,[15,66] an empirical equation proposed by Kurokawa[68] was used to transform the measured complete mixing time to melt the circulation rate. Figures 5 and 6 show the calculated circulation rate and gas-holdup distribution in the plume zone at different gas flow rates, respectively. As illustrated in Fig. 5, the present simulation nearly catches up to the values measured by Park,[15,66] although a slightly larger error was
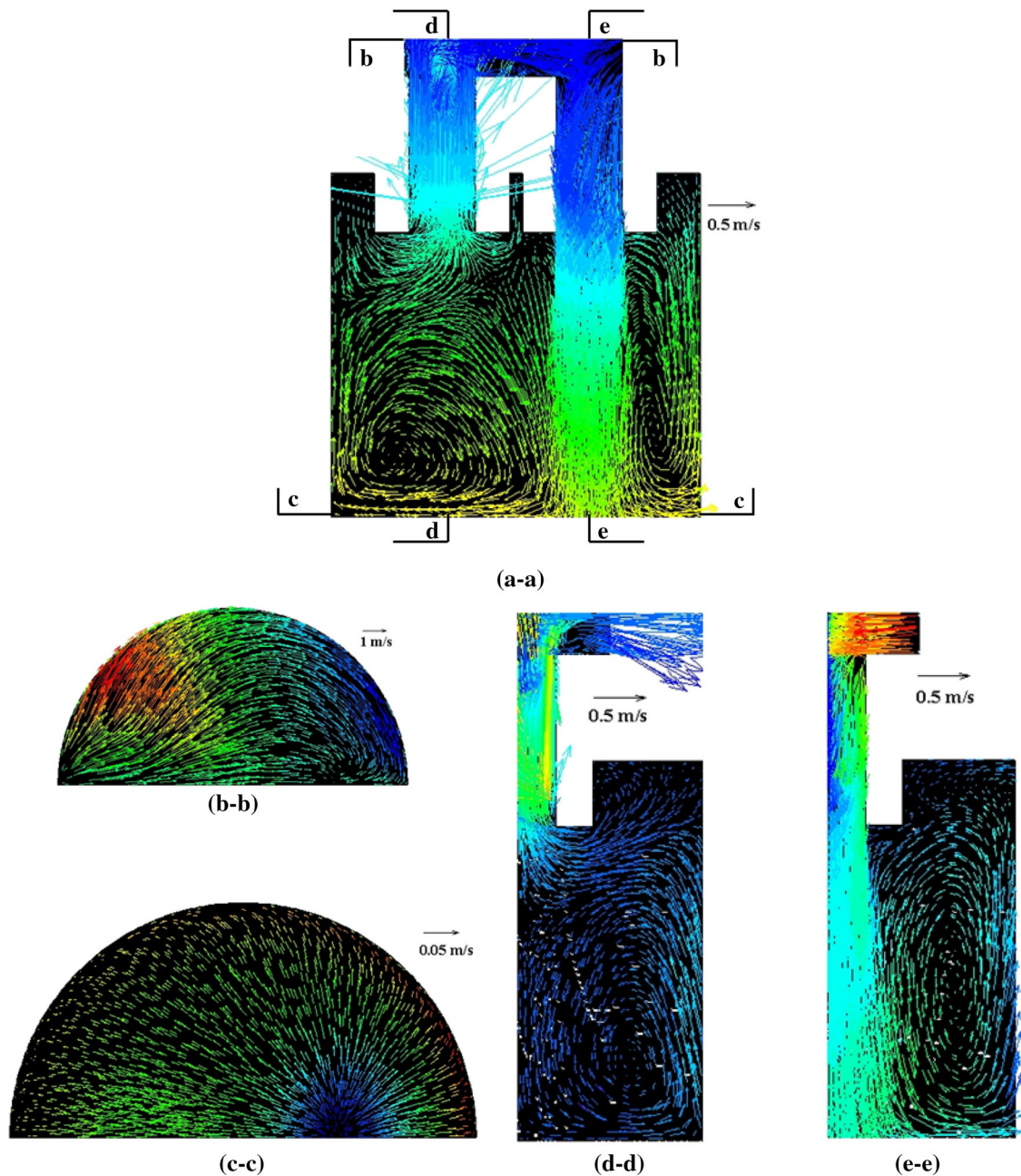
Fig. 3. Velocity vectors of different sections in actual RH. Section (a-a) is the symmetry plane ($y = 0$ mm plane) of the RH reactor, and the positions of sections (b-b), (c-c), (d-d) and (e-e) are indicated in section (a-a).

observed at the gas flow rate of 210 Nm³/h, which possibly resulted from the estimation of bubble expansion in present work, or a larger time interval for sampling in their experiment. In addition, it also can be observed in Fig. 5 that the circulation rate increases markedly with the increase in gas flow rate, and it does not increase much when the flow rate increases beyond 210 Nm³/h. With a further increasing gas flow rate, the circulation rate increases slowly and then reaches a constant. This tendency can be explained as follows: As the gas flow rate increases to 210 Nm³/h, the plume volume and contact area between bubbles and melt increase

rapidly (Fig. 6a, b, and c), leading to enhancing the circulation rate. Further increasing the gas flow rate to 270 Nm³/h, the plume volume and contact area changes a little (Fig. 6c and d) so that the circulation rate remains approximately constant. This result in the present work corresponds with the experimental result of many investigators[9,22,34,36,37,67] but is contrary to the simulated result of Geng[31] and Park.[66] In the simulated result of Geng[31] and Park,[66] when the circulation flow rate exceeds the maximum, it has an evident tendency to decrease. The reason is possibly due to the overestimated plume volume or gas penetration depth in a
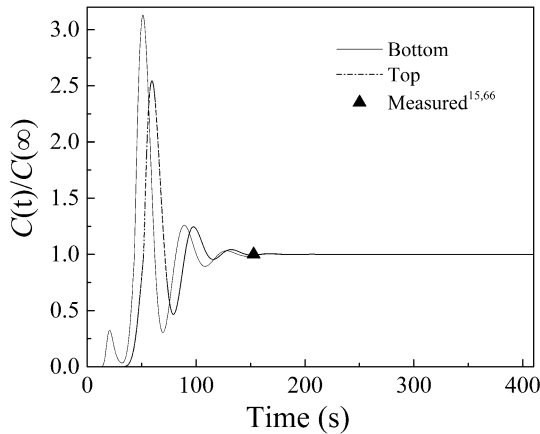
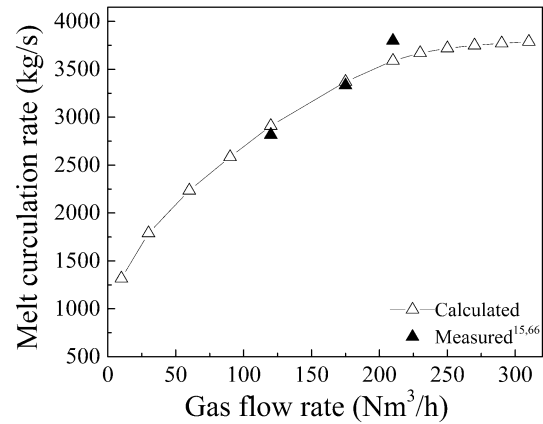Fig. 4. Variation of tracer concentration with time.

Fig. 5. Variation of circulation rate as a function of argon flow rate.

homogeneous fluid model at a high gas flow rate, which occupies too much space in the up-snorkel and retards the liquid flow.

The local liquid velocity was verified by using water modeling because it is almost impossible to measure for melt. Wei[67] measured the local velocity at several locations with a 1/5-scale water model of a 90-ton RH reactor, and the circulation rate at different lifting gas flow rates was also measured directly, as shown in Table II and Fig. 7, respectively. The comparisons indicated that the predicted local velocity and circulation rate agree with the experimental data within experimental error.

It could be concluded that the multiphase flow in both the actual RH reactor and the water model could be reasonably predicted by the present model. In the following sections, the effects of the initial diameter and expansion of the bubble, as well as the various interphase forces on the multiphase flow of the RH reactor, are discussed briefly.

Importance of Initial Diameter and Expansion of the Bubble

The effects of the initial diameter and bubble expansion on the melt circulation rate are shown in Fig. 8 when the gas flow rate is 120 Nm^3/h. It can be found that by increasing the bubble diameter from 10 mm to 20 mm, the circulation rate decreases slowly. This is because with increasing the bubble diameter, the plume volume changes little and the contact area between bubbles and the melt will slightly decrease. As a result, the changes in the bubble diameter within the above ranges have a negligible effect on the melt circulation rate.

Figure 8 also indicates that bubble expansion has a strong impact on the melt circulation rate. The circulation rate without considering bubble expansion is almost half of the actual value. As shown in Fig. 9, the bubble expands rapidly in the initial stage of rising mainly due to the sudden increase of temperature inside the bubble, and after that, the bubble continues to expand as a result of pressure
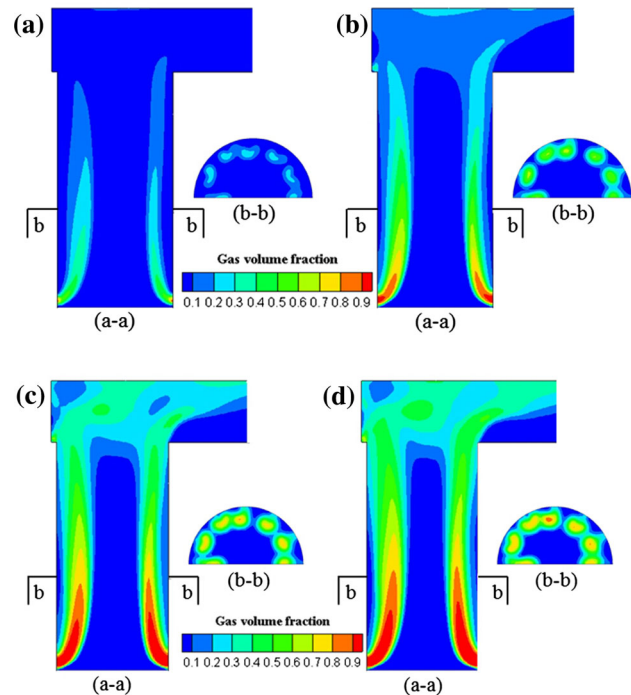

Fig. 6. Gas-holdup distribution at the plane of symmetry (a-a) and the cross-section of up-snorkel (b-b) in plume zone ((a) Q_g = 30 Nm^3/h; (b) Q_g = 90 Nm^3/h; (c) Q_g = 210 Nm^3/h; (d) Q_g = 270 Nm^3/h).

drop. At last, the bubble diameter near the surface of the vacuum chamber doubles the initial diameter at the nozzle. Figure 10 shows the effect of bubble expansion on gas-holdup distribution in the plume zone. Clearly, the plume volume and contact area between bubbles and melt without considering the bubble expansion is much smaller than that when the expansion is considered. Therefore, bubble expansion must be taken into account to reasonably describe the multiphase flow in an actual RH reactor.

Table II. Liquid velocity at different positions (Q_g = 1.9 Nm³/h)

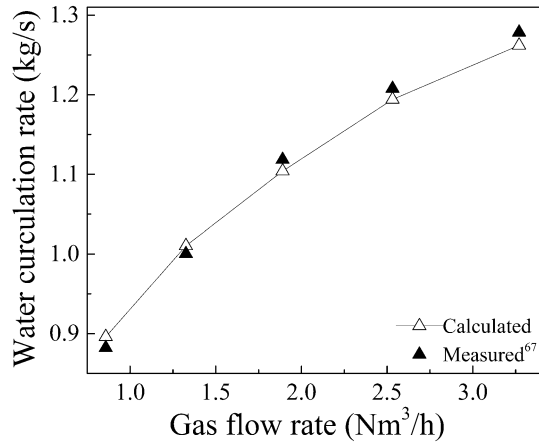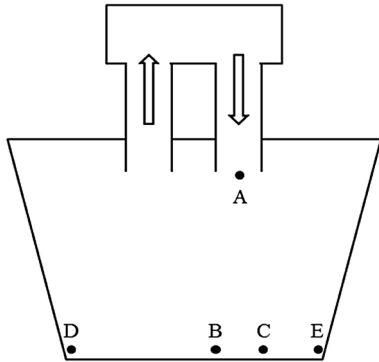| Position		Measured (m/s)[67]	Predicted (m/s)
	A: Outlet of down-snorkel	0.452	0.437
	B: Impinged zone on the bottom	0.245	0.231
	C: Impinged zone on the bottom	0.28	0.27
	D: Ascending stream along the ladle wall	0.12	0.112
	E: Ascending stream along the ladle wall	0.163	0.157

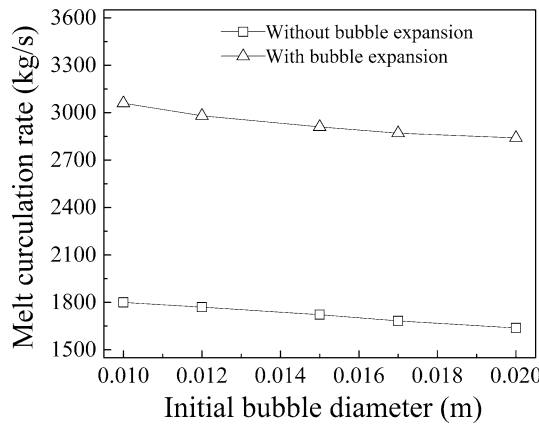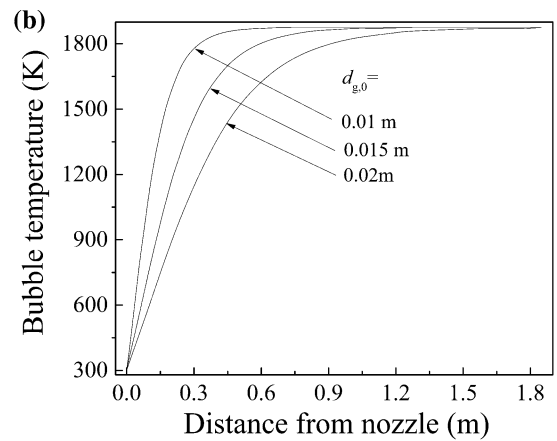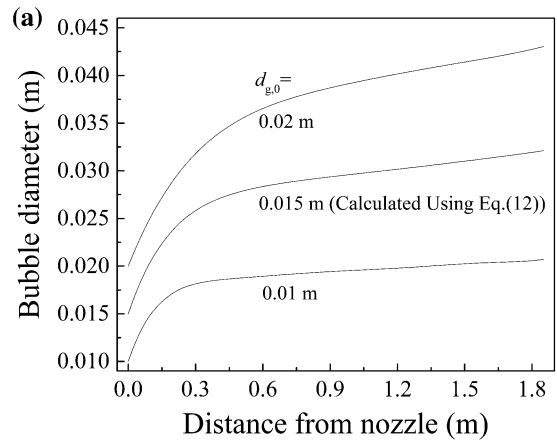Fig. 7. Changes in circulation rate with different gas flow rates.

Fig. 8. Effect of initial diameter and expansion of bubble on circulation rate.

Fig. 9. Changes of diameter (a) and temperature (b) of bubble during rising.
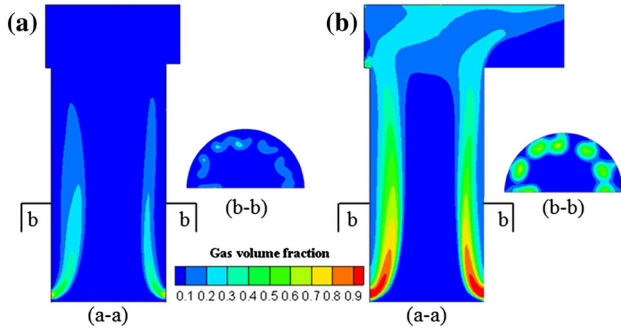
Fig. 10. Effect of bubble expansion on gas-holdup at $Q_g = 120$ Nm^3/h ((a) without bubble expansion; (b) with bubble expansion).

Importance of Various Interphase Forces

In viscous gas–liquid fluid, drag force always exists when a bubble moves relative to the liquid. Generally, the drag force is the dominant contribution to the interaction forces and plays an absolutely essential role in determining the multiphase flow. However, the influence of nondrag forces (lift force, virtual mass force, and the turbulent dispersion force) may also or may not be important depending on the actual fluid flow. Therefore, the drag force is considered in all cases. Figure 11 shows the influence of various interphase forces on the liquid circulation rate. The result indicates that the drag force plays a decisive role in determining the circulation rate, and the turbulent dispersion force also has a strong impact on the circulation rate, while the lift force and virtual mass force do not have an obvious effect on it. It can be believed that the prediction without considering turbulent dispersion force only accounts for 75–85% of the actual value. This was also the reason why the predicted circulation rate was consistently less than 15–20% of the measurement, as reported by Kishan et al.[35] As a result, the turbulent dispersion force should be responsible for successful prediction of multiphase flow in the RH reactor. However, this force was neglected by most of the researchers.[22,33–37,40,41]

Because the multiphase flow is determined by a plume structure in the RH reactor, the effect of turbulent dispersion force on gas-holdup should be clarified, as shown in Fig. 12. When the turbulent dispersion force is absent (Fig. 12a), the gas blown into the melt rises directly along the wall of the up-snorkel, and the plume size is narrow. This phenomenon is called the gas-adhering wall effect, and it exists in the simulation results of most studies based on the Euler–Euler approach.[22,33–37] However, this phenomenon is not in agreement with the observation, as reported by Parreiras et al.[36,37] In their water modeling, as the gas rate increased gradually, the plume zone tended to concentrate in the central area of the up-snorkel, creating a region that was predominantly occupied by bubbles. As shown in Fig. 12b, the gas-adhering wall effect disappears when turbulent dispersion force is
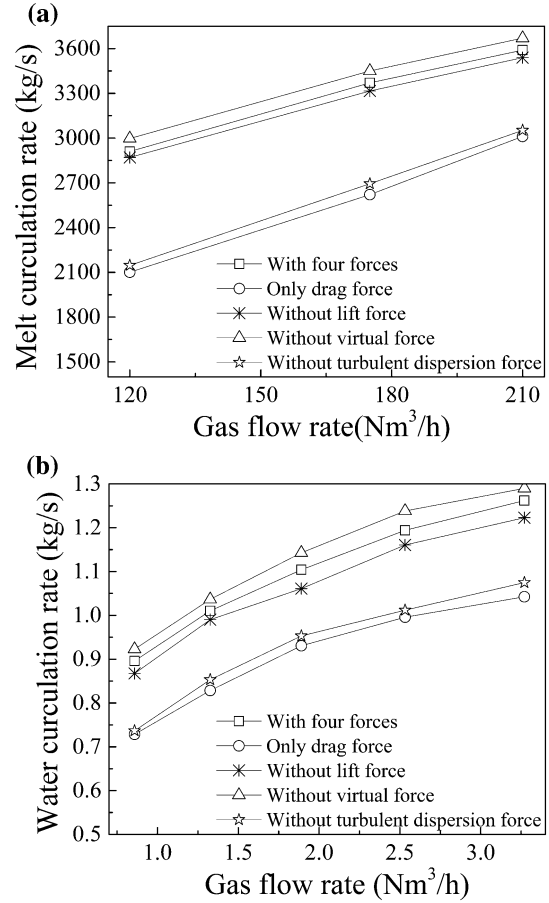

Fig. 11. Effect of interphase forces on circulation rate ((a) actual RH reactor; (b) water model).
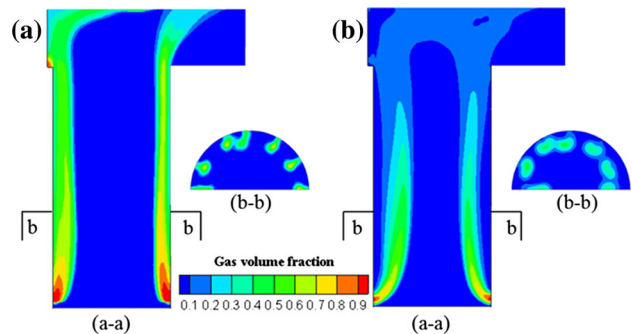

Fig. 12. Effect of turbulent dispersion force on gas-holdup at $Q_g = 60$ Nm^3/h ((a) without turbulent dispersion force; (b) with turbulent dispersion force).

present because this force plays a decisive role in driving the bubbles away from the wall toward the center of the snorkel. In addition, when this force is considered, the plume zone produces dispersion and plume size increases obviously, due to the fact that the effect of liquid velocity fluctuation on bubble motion is considered. Hence, the turbulent dispersion force should be the key to reasonably predicting the plume structure in the RH reactor and must be considered.

CONCLUSION

In the present work, a mathematical model was developed to investigate the RH reactor by using the Euler–Euler approach, and four interphase forces between the gas and liquid phases were considered. Meanwhile, the bubble expansion due to thermal and pressure effects was also taken into account for the actual RH reactor. The following conclusions were derived:

1. Numerical results of circulation rate, local liquid velocity, and mixing time agree well with the measurements, so the multiphase flow in both the actual RH reactor and water model can be reasonably predicted by using the present model.
2. The initial bubble diameter has a weak impact on multiphase flow, but the bubble expansion has a tremendous impact on it for the actual RH reactor.
3. The drag force and turbulent dispersion force strongly influence the multiphase flow in the RH reactor, while the lift force and virtual mass force only have negligible influence on it.
4. Increasing the gas flow rate initially enhances the circulation rate, but the tendency is not obvious beyond a certain level.

REFERENCES

1. K. Shirabe and J. Szekely, *Trans. ISIJ.* 23, 465 (1983).
2. V. Seshadri and S.L. De Souza, *Trans. ISIJ.* 26, 133 (1986).
3. K. Yamaguchi, Y. Kishimoto, T. Sakuraya, T. Fujii, M. Aratani, and H. Nishikawa, *ISIJ Int.* 32, 126 (1992).
4. Y. Miki, B.G. Thomas, A. Denissov, and Y. Shimada, *Ironmaker Steelmak.* 24, 31 (1997).
5. L.F. Zhang and F. Li, *JOM* 66, 1227 (2014).
6. K. Nakanishi, J. Szekely, and C.W. Chang, *Ironmaker Steelmak.* 2, 115 (1975).
7. S.K. Ajmani, S.K. Dash, S. Chandra, and C. Bhanu, *ISIJ Int.* 44, 82 (2004).
8. T. Kuwabara, K. Umezawa, K. Mori, and H. Watanabe, *Trans. ISIJ.* 28, 305 (1988).
9. C. Kamata, S. Hayashi, and K. Ito, *Tetsu to Hagané* 84, 484 (1998).
10. R. Tsujino, J. Nakashima, M. Hirai, and I. Sawada, *ISIJ Int.* 29, 589 (1989).
11. M. Szatkowski and M.C. Tsai, *Ironmaker Steelmak.* 18, 65 (1991).
12. Y. Kato, H. Nakato, T. Fujii, S. Ohmiy, and S. Takator, *ISIJ Int.* 33, 1088 (1993).
13. B.K. Li and F. Tsukihashi, *ISIJ Int.* 40, 1203 (2000).
14. Y.G. Park and K.W. Yi, *ISIJ Int.* 43, 1403 (2003).
15. Y.G. Park, K.W. Yi, and S.B. Ahn, *ISIJ Int.* 41, 403 (2001).
16. Y.S. Chen, Y.D. He, D.Q. Cang, and Z.Z. Huang, *Int. J. Min. Metall. Mater.* 8, 259 (2001).
17. M.Y. Zhu, J. Sha, and Z.Z. Huang, *Acta Metall. Sin.* 36, 1175 (2000).
18. B.K. Li and F. Tsukihashi, *ISIJ Int.* 45, 972 (2005).
19. M.Y. Zhu, Y.L. Wu, C.W. Du, and Z.Z. Huang, *J. Iron Steel Res. Int.* 12, 20 (2005).
20. A.H. Castillejos and J.K. Brimacombe, *Metall. Trans. B* 18B, 659 (1987).
21. M. Iguchi, H. Kawabata, K. Nakajima, and Z. Morita, *Metall. Mater. Trans. B* 26B, 67 (1995).
22. J.H. Wei and H.T. Hu, *Chin. J. Process Eng.* 6S1, 62 (2006).
23. N.J. Themelis, P. Tarassoff, and J. Szekely, *Trans. Metall. Soc. AIME.* 245, 2425 (1969).
24. C.L. Chen, J.Y. Zhang, B. Du, and T.P. Zhou, *Trans. Nonferrous Met. Soc. China* 11, 950 (2001).
25. P.A. Kishan and S.K. Dash, *ISIJ Int.* 49, 495 (2009).
26. V.V. Buwa, D.S. Deo, and V.V. Ranade, *Int. J. Multiph. Flow* 32, 864 (2006).
27. D. Darmana, N.G. Deen, and J.A.M. Kuipers, *Chem. Eng. Sci.* 60, 3383 (2005).
28. J. Zhou, J.M. Zhou, Z. Chen, and Y.N. Mao, *JOM* 66, 1629 (2014).
29. V.V. Buwa and V.V. Ranade, *AIChE J.* 50, 2394 (2004).
30. W.T. Lou and M.Y. Zhu, *Metall. Mater. Trans. B* 44B, 1251 (2013).
31. D.Q. Geng, H. Lei, and J.C. He, *Metall. Mater. Trans. B* 41B, 234 (2010).
32. M. Cournil, F. Gruy, and P. Gardin, *Proceedings of the Computational Modeling of Materials, Minerals and Metals Processing* (San Diego, California, 2001), pp. 139–148.
33. J.H. Wei and H.T. Hu, *Ironmaker Steelmak.* 32, 427 (2005).
34. J.H. Wei and H.T. Hu, *Chin. J. Process Eng.* 6S1, 66 (2006).
35. P.A. Kishan and S.K. Dash, *Int. J. Numer. Method H* 16, 890 (2006).
36. A.A. Nascimento and R.P. Tavares, *Iron & Steel Technology Conference* (St. Louis: AISTech, 2009), pp. 897–906.
37. L. Neves, C.A.R. Carneiro, R.F. Reis, and R.P. Tavares, *Comput. Methods Mater. Sci.* 10, 207 (2010).
38. F.S. Qi, L. Yang, B.K. Li, and T. Fumitaka, *J. Iron Steel Res. Int.* 18S2, 176 (2011).
39. F.S. Qi, L. Yang, H.J. Liu, and B.K. Li, *J. Iron. Steel Res. Int.* 19, 888 (2012).
40. J.H. Wei and H.T. Hu, *Steel Res. Int.* 77, 32 (2006).
41. J.H. Wei and H.T. Hu, *Steel Res. Int.* 77, 91 (2006).
42. M.E. Diaz, A. Iranzo, D. Cuadra, R. Barbero, F.J. Montes, and M.A. Galan, *Chem. Eng. J.* 139, 363 (2008).
43. A.A. Basheer and P. Subramaniam, *Chem. Eng. J.* 187, 261 (2012).
44. D.Q. Geng, H. Lei, and J.C. He, *Ironmaker Steelmak.* 39, 431 (2012).
45. S. Mats (Doctoral thesis, Royal Institute of Technology, 2004).
46. M.J. Prince and H.W. Blanch, *AIChE J.* 36, 1485 (1990).
47. H. Luo and H.F. Svendsen, *AIChE J.* 42, 1225 (1996).
48. A. Alexiadis, *Appl. Math. Model.* 31, 1534 (2007).
49. L. Schiller and Z. Naumann, *Zeit. Ver. Deutsch. Ing.* 77, 318 (1935).
50. A.R. Banderas, R.D. Morales, L.G. Demedices, and M.D. Cruz, *ISIJ Int.* 43, 653 (2003).
51. P. Chen, J. Sanyal, and M.P. Dudukovic, *Chem. Eng. Sci.* 59, 5201 (2004).
52. H. Türkoğlu and B. Farouk, *Metall. Trans. B* 21B, 771 (1990).
53. H. Anglart, O. Nylund, N. Kurul, and M.Z. Podowski, *Nucl. Eng. Des.* 177, 215 (1997).
54. B.L. Smith, *Appl. Math. Model.* 22, 773 (1998).
55. O. Simonin and P.L. Viollet, *Phenomena in Multiphase Flows* (Washington, DC: Hemisphere Publishing Corporation, 1990).
56. O. Simonin and P.L. Viollet, *Numer. Method Multiph. Flows FED* 91, 65 (1990).
57. S.T. Johansen and F. Boysan, *Metall. Trans. B* 19B, 755 (1988).
58. M. Sano, K. Mori, and T. Sato, *Tetsu to Hagané* 63, 2308 (1977).
59. F. Jiang and G.G. Cheng, *Ironmaker Steelmak.* 39, 386 (2012).
60. M. Sano, K. Mori, and Y. Fujita, *Tetsu to Hagané* 65, 1140 (1979).
61. J. Szekely and S.D. Fang, *Metall. Trans.* 5B, 1429 (1974).
62. J. Szekely and G.P. Martins, *Trans. Met. Soc. AIME.* 245, 629 (1969).
63. V.G. Levich, *Physicochemical Hydrodynamics* (Englewood Cliffs: Prentice-Hall Inc., 1962).

64. P.V. Danckwerts, *Gas-Liquid Reactions* (Great Britain: McGraw-Hill Book Company, 1970).

65. N.B. Vargaftik, *Handbook of Physical Properties of Liquid and Gases*, 2nd ed. (Berlin: Springer, 1975).

66. Y.G. Park, W.C. Doo, K.W. Yi, and S.B. An, *ISIJ Int.* 40, 749 (2000).

67. J.H. Wei, N.W. Yu, Y.Y. Fan, S.L. Yang, J.C. Ma, and D.P. Zhu, *J. Shanghai Univ. Engl. Ed.* 6, 167 (2002).

68. N. Kurokawa, *Proc. 5th Int. Conf. for Licenses of the Rh Process* (Vienna, Duisburg: Thyssen Stahl Aktiengesellschaft, 1987), p. 61.